Supporting Information

Synthesis of robust yet flexible and transparent CPA hydrogels inspired by molting crab shells

*Yamei Zao[a], Muqiu You[a], Jieru Ma[a], Xiaoyu Du[a], Yongcan Jin[b], Dagang Li[a], Zhaoyang Xu[a], and Chuchu Chen[a,b]**

[a] College of Materials Science and Engineering, Jiangsu Co-Innovation Center of Efficient Processing and Utilization of Forest Resources, Nanjing Forestry University, Nanjing, Jiangsu 210037, China

[b] College of Light Industry and Food Engineering, Nanjing Forestry University, Nanjing, Jiangsu 210037, China

* Corresponding author: chuchu chen

E-mail address: chuchu_chen@njfu.edu.cn

The Supporting Information file includes:

Fig. S1 to S15

Table S1 to S3

Video S1 to S2

Characterization

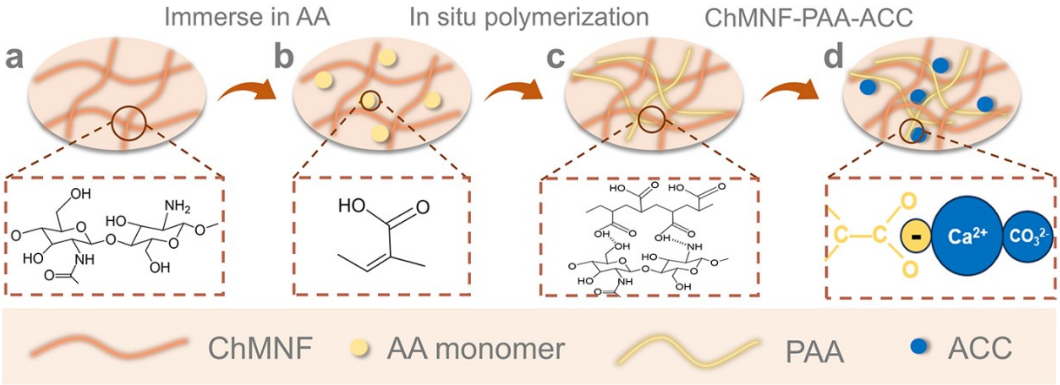

Fig. S1. The preparation process and chemical reaction scheme of CPA hydrogel.

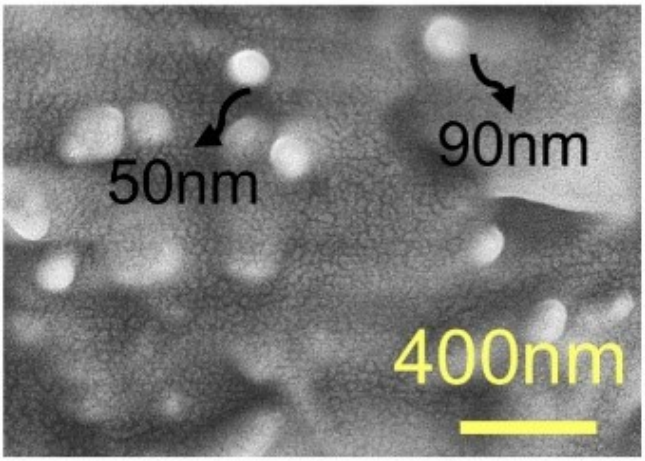

Fig. S2. Cross-sectional SEM images of CPA-1. ACC in CPA-1 were spherical nanoparticles with a 50-90 nm diameter.

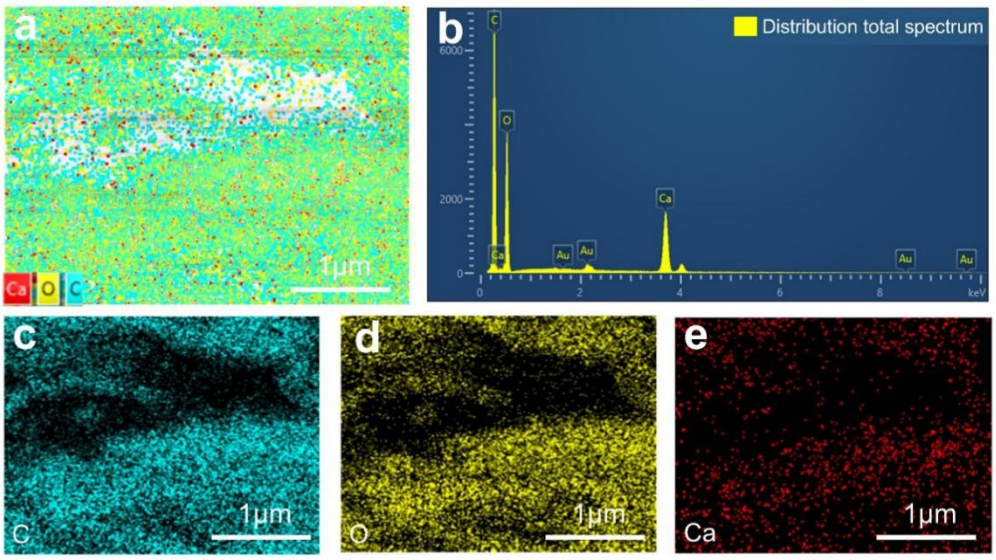

Fig. S3. (a,c-d) EDS diagram of C, O, and Ca elements of CPA-16 (Fig. 2k). (b) Spectrum of total element distribution.

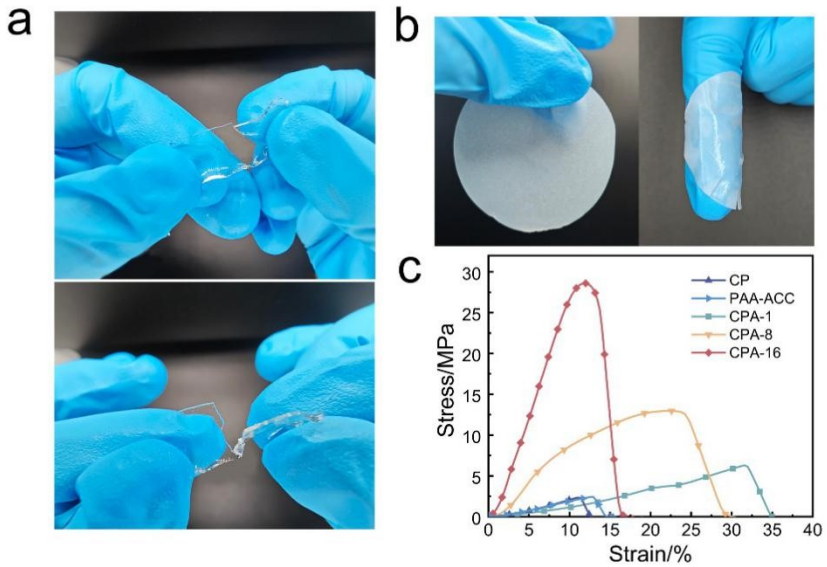

Fig. 4. (a) The hydrogel-PAA as a control. The mechanical strength of PAA hydrogel was too weak to be measured. (b) The hydrogel-ChMNF as a control. The mechanical strength of ChMNF hydrogel was too weak to be measured. (c) Stress-strain curves of control hydrogels and CPA hydrogels.

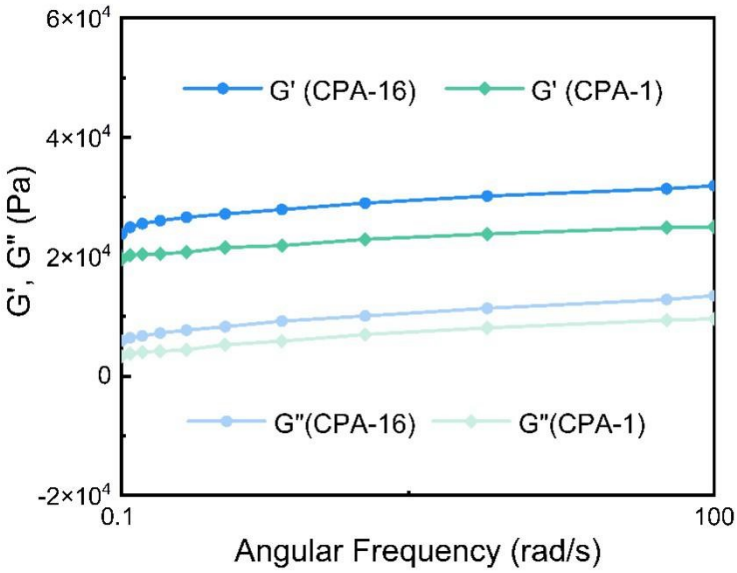

Fig. S5. Dynamic viscoelastic properties of CPA-16 hydrogel at 25 °C.

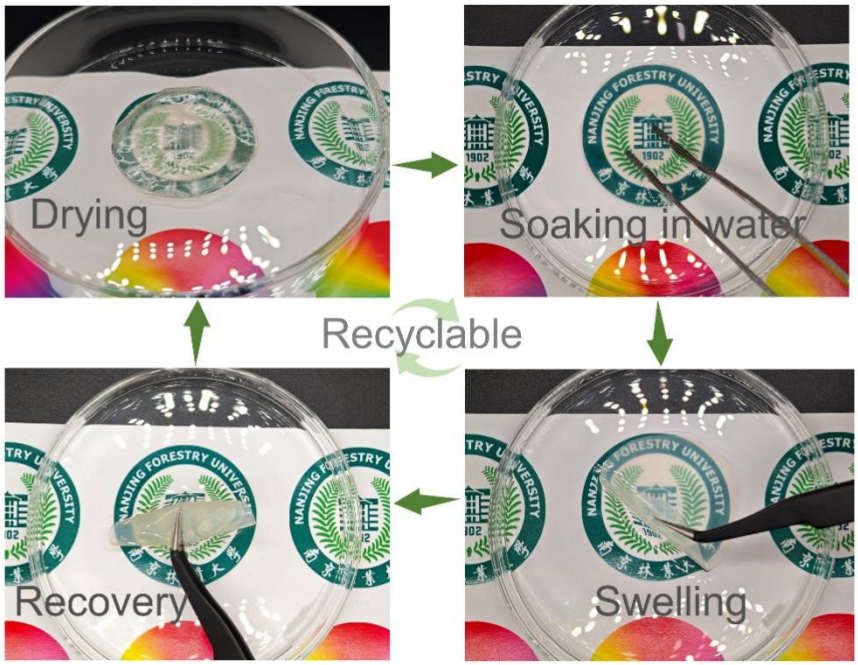

Fig. S6. The drying-swelling processes of CPA hydrogel. After air drying, the CPA film could be recovered into hydrogel totally and recycled easily after soaking in water.

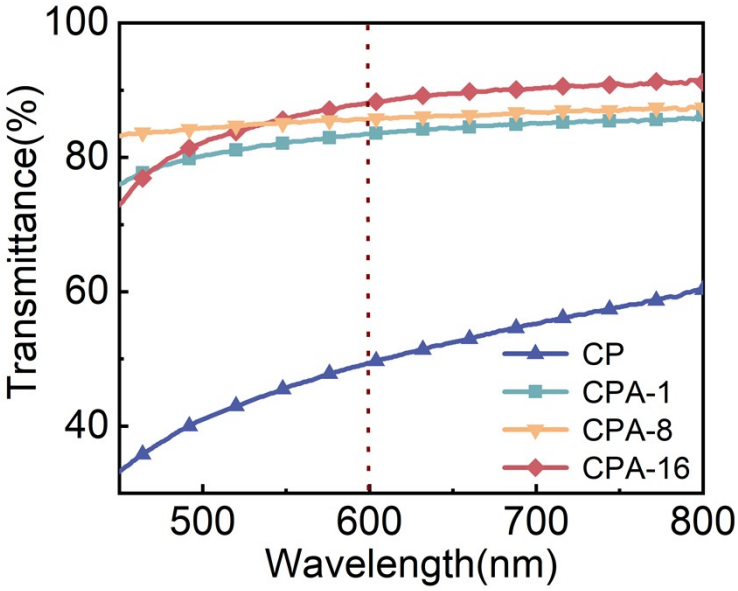

Fig. S7. The light transmittance of CP and CPA-n.

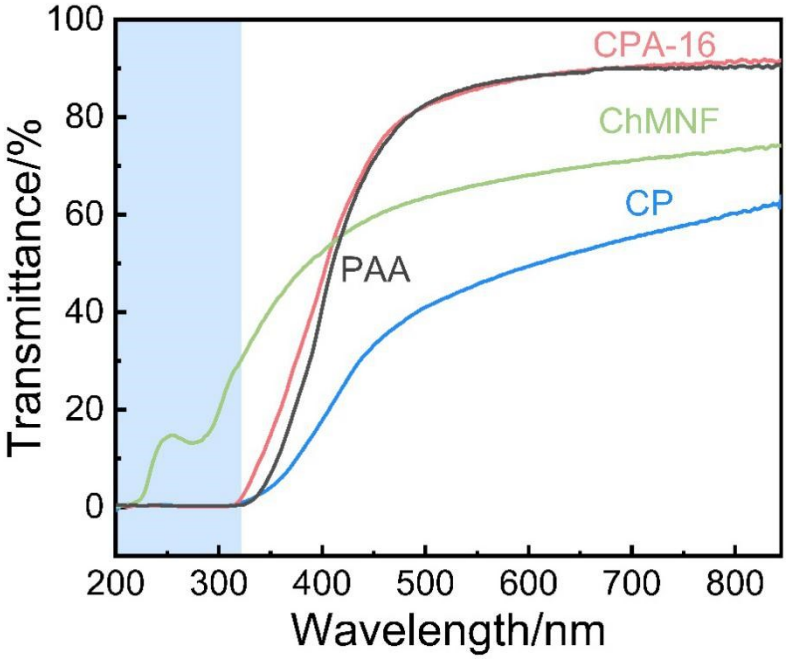

Fig. S8. The light transmittance of ChMNF, PAA, CP and CPA.

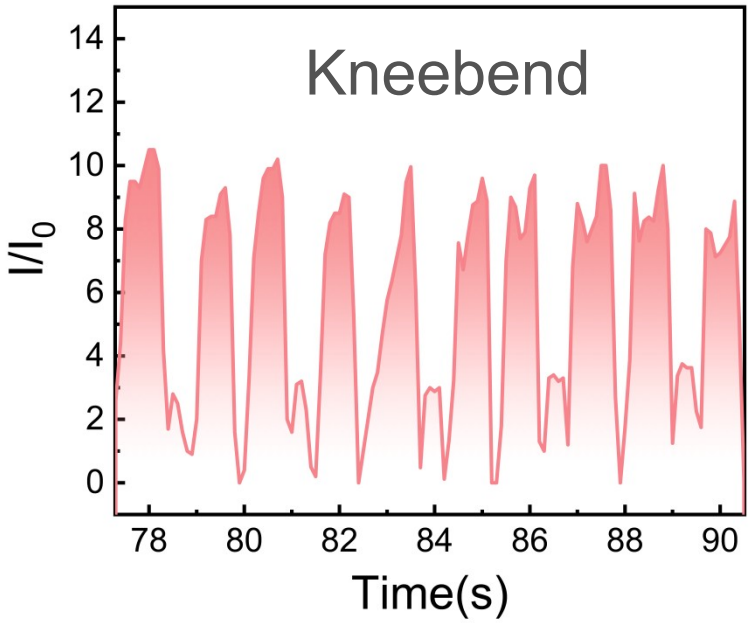

Fig. S9. CPA-based sensor was used to detect the motion of kneebend.

Fig. S10. CPA-based sensor was used to detect saying “Nanjing”.

Fig. S11. CPA-based sensor responds to temperature by observing signal changes under controlled ambient temperature conditions.

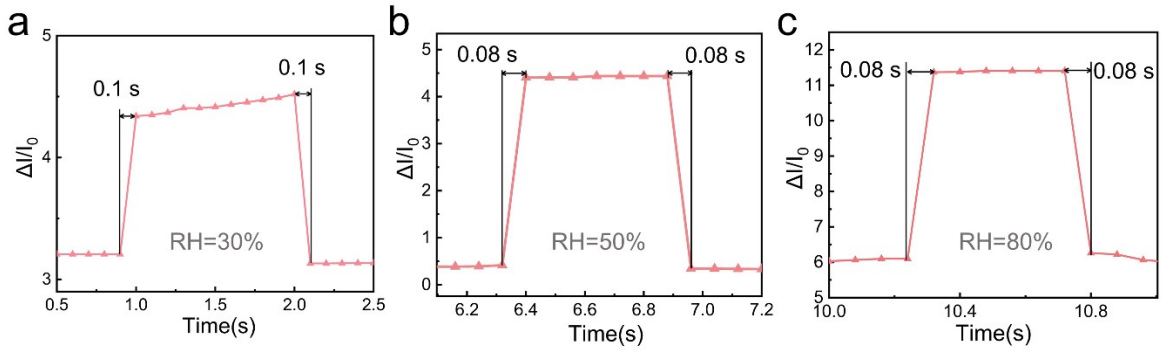

Fig. S12. Response time of CPA-based sensor with different humidity.

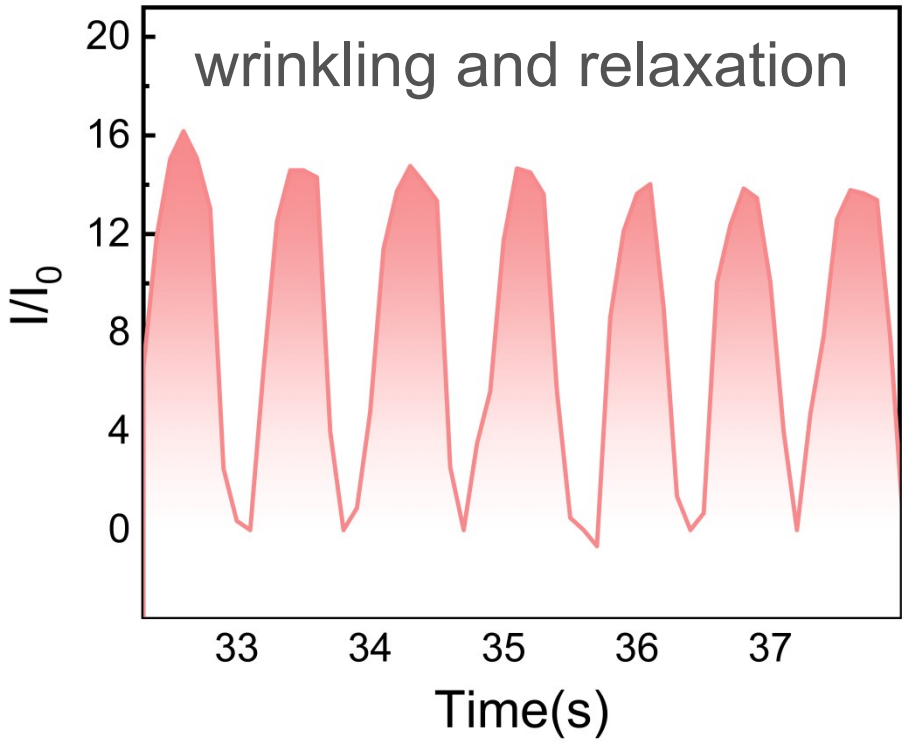

Fig. S13. CPA-based sensor was applied to repetitive wrinkling and relaxation on the eyebrow.

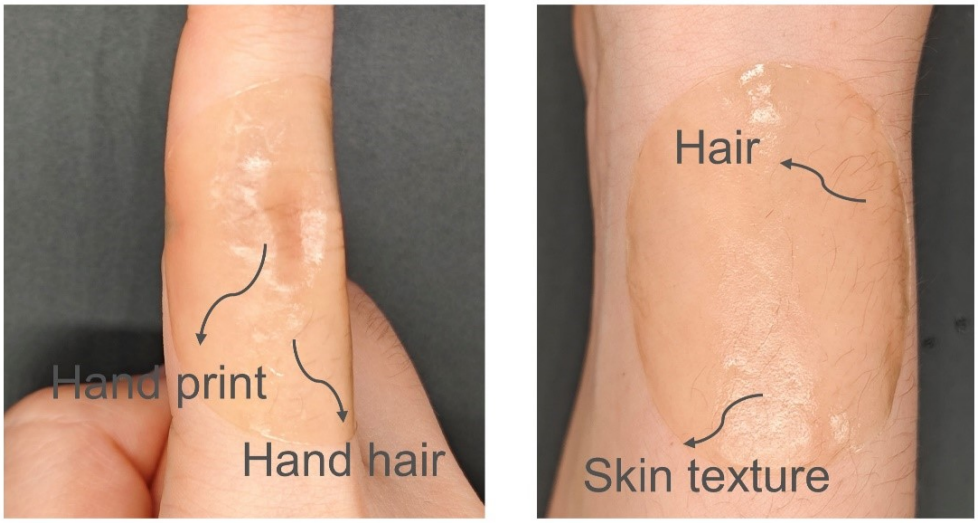

Fig. S14. CPA hydrogel was highly transparent and soft-and-thin, it could be even seen the hair, hand prints, and skin texture underneath the sample.

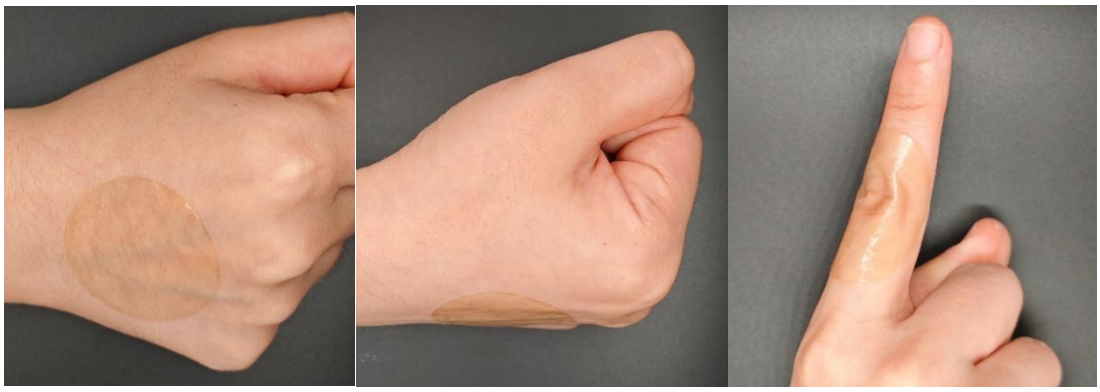

Fig. S15. CPA hydrogel was well-compatible with human body curves.

Table S1. Comparison of light transmittance and tensile strength with the reported hydrogels

Samples	Reference	Transmittance at 600nm (%)	Tensile strength (MPa)
IC hydrogel	[1]	90	0.4
PAMC	[2]	87.5	0.05
CMCS-Ca^{2+}/PAAm/PNMA	[3]	90	2.65
DN-hydrogel	[4]	27-89	1.73
HFMOS	[5]	-	9.33
anisotropic hydrogel	[6]	-	12.8
Our work (CPA)	-	**88.1**	**28.6**

Table S2. Mechanical properties of CP and CPA hydrogels.

Samples	Tensile strength (MPa)	Elongation at Break (%)	Young's modulus (MPa)
CP	2.34±0.14	11.03±3.48	20.81±0.29
CPA-1	6.3±0.70	31.6±4.22	15.02±0.25
CPA-4	9.27±2.75	25.87±3.19	31.63±0.20
CPA-8	12.96±2.26	22.01±2.30	48.23±0.74
CPA-12	15.87±2.06	18.85±2.23	188.17±2.53
CPA-16	28.60±0.66	12.00±5.50	310.30±2.06
CPA-24	23.66±2.39	8.34±1.68	349.85±4.48

Table S3. Comparison of response and recovery time with the reported hydrogels.

Samples	Reference	Response time (ms)	Recovery time (ms)
PACT-P	[7]	200	200
PPGP	[8]	169	198
PAMC	[9]	216	227
cellulose/PEDOT:PSS	[10]	350	176
s-PCT hydrogels	[11]	200	-
Gel/P(AM-co-AMPS)	[12]	350	290
$HDES_{EG}/CCNF_{3\%}$	[13]	375	500
IC hydrogel	[1]	180	170
Our work (CPA)	**-**	**80**	**80**

Video S1. CPA hydrogel is flexible and possesses good fatigue resistance along with rapid recovery from deformation.

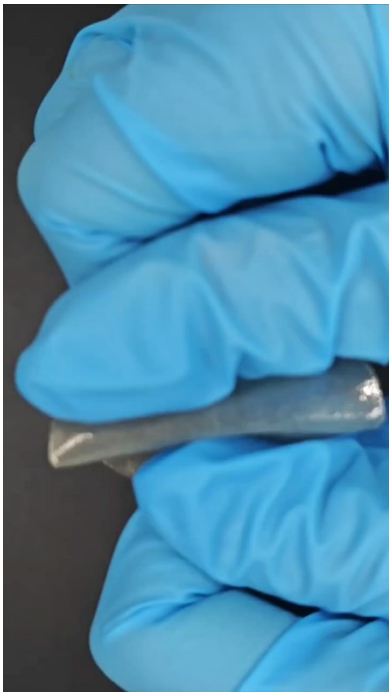

Video S2. CPA hydrogel is flexible enough to be folded into various shapes repeatedly.

Characterization

Morphology Observation. The morphological features of ChMNF, CP, and CPA samples were measured using an emission scanning electron microscope (FE-SEM, Regulus 8100, Hitachi, Japan). The dried sample was sprayed with gold by an automatic gold spraying instrument before test, and the scanning voltage was set to 2 kV. The FE-SEM was equipped with an EDS instrument (OXFORD Ultim Max 170, UK).

Fourier Transform Infrared (FTIR) Characterization. The chemical characterization of the prepared ChMNF, CP, and CPA samples were characterized using a Fourier transform infrared spectrometer (NICOLET IS10, Thermo Scientific, Inc). These samples were dried first and then cut into pieces to expose the inner sides for testing. The scanning range of the infrared spectrum was set between 500-4000 cm^{-1} with a resolution of 4 cm^{-1}.

X-ray Diffraction (XRD) Measurement. An X-ray diffractometer (2036E202, Rigaku Corporation, Japan) was used to characterize the crystalline structure of ChMNF, CP, and CPA samples. The specific test conditions were set to 40 kV and 300 mA, and the scanning speed was 5°/min. The diffraction patterns in the scanning angle range of 2θ from 5 to 30° were recorded. The equation of the crystallinity is as follows:

$$CrI = \frac{I - I_{am}}{I} \quad (1)$$

where *CrI* represents the relative degree of crystallinity, *I* is the highest value between 2θ = 19−20°, and I_{am} is the lowest peak of the X-ray diffraction (XRD) pattern.[14]

Thermogravimetric (TG) Analysis. A thermogravimetric analyzer (TG; Q50, TA Instruments) was used to measure the thermal degradation of samples. The heating rate was set at 10 °C/min from 25 to 850 °C under a nitrogen atmosphere.

Differential scanningcalorimetry(DSC) measurement: DSC measurement was conducted on a differential scanning calorimeter (NETZSCH DSC 204F1 Phoenix) from 25 to 250 ℃ at a rate of 10 ℃ min^{-1} under nitrogen flow.

Tensile Test. The mechanical properties of samples were tested by a universal mechanical testing machine (SANS, Shenzhen Xinsansi Material Testing Co., Ltd.), utilizing a 1 kN load cell at a crosshead speed of 40 mm/min. All specimens had a size

of 30 mm × 5mm with a thickness of around 0.1 mm. All data were reported as the average value from measurements of five specimens.

Rheological measurement. Viscoelastic measurements were measured using an advanced rheometer (MARS60). Specifically, the hydrogels were made into a wafer with a diameter of 25 mm and a thickness of 2.5 mm. We performed frequency sweep tests at 1% strain with a testing temperature of 25 °C, covering a range from 0.1 to 100 rad/s.

Optical Measurement. The transmittance and haze of the samples were characterized by an ultraviolet-visible near-infrared spectrophotometer (U-4100, HITACHI, Japan). During the test, the wavelength range was set between 200 and 850 nm, and the scanning speed was 300 nm/min. The T_{UVB} (280-320 nm), T_{UVC} (200-280 nm) of CPA were calculated by Eqs. (2) and (3)[15]

$$T_{UVB} = \frac{\int_{280}^{320} T_{\lambda} \times d\lambda}{\int_{280}^{320} d\lambda} \quad (2)$$

$$T_{UVC} = \frac{\int_{200}^{280} T_{\lambda} \times d\lambda}{\int_{200}^{280} d\lambda} \quad \#(3)$$

where T_{λ} is the average spectral transmittance, d(λ) is the bandwidth, and λ is the wavelength. The blocking percentages for UVB and UVC were calculated by Eqs. (4) and (5)

$$UVB\ blocking = 100\% - T_{UVB} \quad (4)$$

$$UVC\ blocking = 100\% - T_{UVC} \quad (5)$$

Sensor Performance. The hydrogel sensor device was attached to human skin or put in a different environment followed by various external stimuli. The electrical resistance changes were tested by a benchtype multimeter (UT-803, UNIT, China) and were simultaneously recorded by a software (UT803 Interface Program version 0.1).

Fluorescence Spectra Analysis. The fluorescence properties of ChMNF, CP, and CPA

samples were characterized by a steady state and transient state fluorescence spectrometer (FluoroMax-4, HORIBA, France) under the excitation of 380 nm. The Front entrance slit was set as a 3.00 nm bandpass.

Reference

1. K. Shen, K. Xu, M. Zhang, J. Yu, Y. Yang, X. Zhao, Q. Zhang, Y. Wu, Y. Zhang and Y. Cheng, *Chem. Eng. J.*, 2023, **451**, 138525.
2. J. L. Gao, X. M. Li, L. A. Xu, M. Q. Yan, H. Bi and Q. Y. Wang, *Carbohydr. Polym.*, 2024, **329**.
3. X. R. Xu, C. B. He, F. Luo, H. Wang and Z. C. Peng, *POLYMERS*, 2021, **13**.
4. J. Yu, C. Dang, H. Liu, M. Wang, X. Feng, C. Zhang, J. Kang and H. Qi, *Macromol. Mater. Eng.*, 2020, **305**, 2000475.
5. H. P. Yu and Y. J. Zhu, *Nano Res.*, 2021, **14**, 3643-3652.
6. S. Wang, L. Lei, Y. Tian, H. Ning, N. Hu, P. Wu, H. Jiang, L. Zhang, X. Luo and F. Liu, *Mater. Horiz.*, 2024, **11**, 2131-2142.
7. W. Wang, X. Deng and C. Luo, *J. Mater. Chem. C*, 2023, **11**, 196-203.
8. S. Kondaveeti, G. Choi, S. C. Veerla, S. Kim, J. Kim, H. J. Lee, U. Kuzhiumparambil, P. J. Ralph, J. Yeo and H. E. Jeong, *Nano Convergence*, 2024, **11**, 12.
9. J. Gao, X. Li, L. Xu, M. Yan, H. Bi and Q. Wang, *Carbohydr. Polym.*, 2024, **329**, 121784.
10. A. F. Wibowo, J. W. Han, J. H. Kim, A. Prameswati, S. A. N. Entifar, J. Park, J. Lee, S. Kim, D. C. Lim and Y. Eom, *ACS Appl. Mater. Interfaces*, 2023, **15**, 18134-18143.
11. W. Wang, X. Deng, Z. Tian and C. Luo, *Eur. Polym. J.*, 2023, **196**, 112277.
12. X. Li, L. Cao and L.-p. Chen, *Biochem. Eng. J.*, 2022, **187**, 108606.
13. Q. Li, B. Tian, G. Tang, H. Zhan, J. Liang, P. Guo, Q. Liu and W. Wu, *J. Mater. Chem. A*, 2024, **12**, 3589-3600.
14. I. F. Nata, S. S.-S. Wang, T.-M. Wu and C.-K. Lee, *Soft Matter*, 2012, **8**, 3522-3525.
15. Q. Feng, L. Wang, Z. Wan, X. Bu, Q. Deng, D. Li, C. Chen and Z. Xu, *Int. J.*

Biol. Macromol., 2023, **250**, 126059.